Minimizing the Concentration of Diblock Copolymer Needed To Organize Blends of Weakly Segregated Polymers by Tuning Attractive and Repulsive Interactions

Megan L. Ruegg,[†] Benedict J. Reynolds,[†,‡] Min Y. Lin,[⊥,#] David J. Lohse,[⊥] and Nitash P. Balsara*[,†,§]

Department of Chemical Engineering, University of California, Berkeley, California 94720; Earth Science Division, Lawrence Berkeley National Laboratory, University of California, Berkeley, California 94720; Materials Sciences Division and Environmental Energy Technologies Division, Lawrence Berkeley National Laboratory, University of California, Berkeley, California 94720; and ExxonMobil Research and Engineering, Annandale, New Jersey 08801

Received June 7, 2006; Revised Manuscript Received September 26, 2006

ABSTRACT: This paper is concerned with the design of A−C diblock copolymer surfactants for stabilizing mixtures of weakly segregated A and B homopolymers. Component A was saturated polybutadiene with 89% 1,2-addition, component B was polyisobutylene, and component C was saturated polybutadiene with 63% 1,2-addition. The C-block exhibits attractive interactions with B and repulsive interactions with A. The effect of the molecular weight and concentration of the A−C block copolymer on the phase behavior of critical A/B mixtures was studied by small-angle neutron scattering. We show that organized microphases are obtained when as little as 1 vol % of the A−C copolymer is added to a 50/50 A/B mixture. In contrast, in the well-studied case of A/B/A−B mixtures, 9 vol % of the A−B diblock copolymer is needed to obtain organized microphases in a 50/50 A/B mixture. Self-consistent-field theory (SCFT) calculations, using independently determined Flory−Huggins interaction parameters and statistical segment lengths, predicted the size of the organized microphases within 10% of the experimental value for most temperatures and concentrations of diblock copolymer. The theoretically predicted phase boundary between organized microphases and macrophase separation was in good agreement with experiments.

1. Introduction

This paper is part of a series on designing A−C diblock copolymer surfactants for A and B homopolymers.[1−5] In previous work, organized microphases were obtained by the addition of an A−C diblock copolymer to critical mixtures of A and B homopolymers. The design of the A−C surfactant is based upon the design of nonionic surfactants in oil/water systems where A is an alkane, B is water, and A−C is an alkyl polyglycol ether molecule.[6−11] In both the polymeric and aqueous systems, the A−C surfactant is designed such that the C-block has attractive interactions with the B homopolymer and repulsive interactions with the A homopolymer. The present study is motivated by other studies in which A−C or C−D copolymers with attractive and repulsive interactions (diblock copolymers, graft copolymers, reactive compatibilization, etc.) are used for compatibilizing A and B homopolymers.[1−5,12−22] Traditionally, the approach has been to use an A−B diblock copolymer to organize A and B homopolymers.[23−55]

One parameter for gauging the effectiveness of a surfactant is the minimum concentration (volume fraction) of that surfactant that is required to organize a given blend of immiscible fluids ($\phi_{s,min}$). In this paper we restrict our attention to weakly segregated 50/50 A/B blends. Previous studies utilizing A−C surfactants have not yet proven that they are more effective than A−B surfactants at reducing the concentration of surfactant needed for creating organized phases.[1−5,12−15] In ref 2, for example, it was shown that $\phi_{s,min} = 0.1$ for A/B/A−C mixtures, which is similar to the result obtained in A/B/A−B mixtures. In this paper we will show that tuning the interactions between the components in A/B/A−C mixtures can lead to a substantial reduction in $\phi_{s,min}$. In fact, the value of $\phi_{s,min}$ obtained in the present study is lower than that of all previous studies on A/B/A−B polymer blends. Our experiments on A/B/A−C blends and previous experiments on A/B/A−B blends are limited to weakly segregated A and B homopolymers. Our studies thus far do not directly address the possibility of designing effective surfactants for highly immiscible polymers.

The phase behavior of A/B/A−C polymer blends depends on the molecular weight of the A and B homopolymers, the molecular weights of the A- and C-blocks of the copolymer, volume fraction of the copolymer, three Flory−Huggins interaction parameters, χ_{AB}, χ_{AC}, and χ_{BC}, and the statistical segment lengths of A, B, and C chains. Because of the vastness of parameter space, it is important to use theoretical calculations to guide the design of A−C surfactants. One of the goals of this paper is to establish a comprehensive theoretical framework for predicting the phase behavior of A/B/A−C polymer blends. We use self-consistent-field theory (SCFT) to describe the properties of organized microphases (lamellar phases and microemulsions), the random phase approximation (RPA) to describe homogeneous phases, and Flory−Huggins theory (FHT) to describe macrophase-separated systems.[4,13,47,56−63] The χ parameters and statistical segment lengths (l) needed to complete the theoretical calculations were determined from small-angle neutron scattering measurements on homogeneous

[†] Department of Chemical Engineering, UCB.
[‡] Earth Science Division, UCB.
[§] Materials Sciences Division and Environmental Energy Technologies Division, UCB.
[⊥] ExxonMobil Research and Engineering.
[#] Present address: NIST Center for Neutron Research, National Institute of Standards and Technology, Gaithersburg, MD 20899.

10.1021/ma0612677 CCC: $37.00
Published on Web 01/23/2007

Table 1. Characterization of Polymers[a]

name	M_w (kg/mol)	N	PDI	ρ (g/mL)	% 1,2-addition	n_D
hPB89(24)	24.1	464	1.01	0.8636	90.4	NA
dPB89(24)	25.3	464	1.01	0.9070	90.4	2.79
PIB(24)	24.0	437	1.05	0.9131	NA	NA
hPBPB(79−66)	78.5−65.4	1510−1263	1.01	0.8639	89.7−63.9	NA
hPBPB(88−93)	88.4−92.9	1699−1797	1.02	0.8629	89.9−65.3	NA
hPBPB(240−192)	240−192	4614−3712	1.06	0.8629	86.5−61.5	NA

[a] M_w is the weight-averaged molecular weight, N is the number of reference volume units per chain based on a reference volume of 100 Å^3, PDI $= M_w/M_n$ where M_n is the number-averaged molecular weight, ρ is the average density, and n_D is the number of deuterium atoms per C_4 repeat unit.

binary blends. The theoretical results are thus compared with experimental results without resorting to adjustable parameters.

2. Experimental Methods

In the A/B/A−C polymer blends, component A was saturated polybutadiene with 89% 1,2-addition (sPB89), component B was polyisobutylene (PIB), and component C was saturated polybutadiene with 63% 1,2-addition (sPB63). A−C diblock copolymers in which one block is sPB89 and the other block is sPB63 are labeled sPBPB. (The prefix "s" stands for "saturated" and is replaced by "h" or "d" when we wish to specify whether the polymer is hydrogenated or deuterated.)

Polybutadiene homopolymers and diblock copolymers were synthesized via anionic polymerization and the C═C double bonds were saturated with hydrogen or deuterium gas per methods described in refs 4 and 5. Polyisobutylene was synthesized via cationic polymerization, also described in refs 4 and 5.

All saturated polybutadiene and polyisobutylene polymers were characterized using known methods[4] to determine the density, weight-averaged molecular weight, polydispersity index, and % 1,2-addition (for the saturated polybutadiene polymers). The characterization parameters are summarized in Table 1 for the polymers used in this study. The composition labels for our samples are based on our targets. Samples wherein the % 1,2 addition deviated more than 2% from the targets were discarded.

Binary and multicomponent polymer blends were created via methods described in ref 4. The samples were pressed between two quartz disks and then annealed at 90 °C for 10 min to erase the effects of the shearing force applied to the sample during pressing. As thermal history can have a large effect on the phase behavior in polymer blends, some of the samples were also prepared and annealed at 35 and 150 °C, which will be described further in the Results section.

Small-angle neutron scattering (SANS) experiments were conducted on the NG7 beamline at the National Institute of Standards and Technology in Gaithersburg, MD.[64] Using standard procedures, raw data were converted to absolute coherent scattering intensity, I, as a function of q ($q = 4\pi \sin(\theta/2)/\lambda$, θ is the scattering angle, λ is the wavelength of the incident beam), after corrections for detector sensitivity, background, empty cell, and incoherent scattering were made, using standard procedures.[65] For the deuterated components, corrections for the nonuniformity of deuterium labeling were made.[66] The upper limit of the SANS sample holder was 200 °C. For all of the SANS data in this paper, the error in I was less than the size of the data points in the vicinity of the peaks that were observed.

Small-angle light scattering (SALS) experiments were conducted with a 10 mW HeNe laser, with wavelength $\lambda_{light} = 633$ nm, directed through samples placed in a temperature-controlled heating unit. Scattered light was focused on a detector in the range of 4.33×10^{-4} nm$^{-1} < q < 1.85 \times 10^{-3}$ nm^{-1} using a beam stop and a focusing lens. (The definition of q given above holds for both light and neutron scattering.) Instrumental details are given in ref 1. The intensity was monitored as a function of time after the sample was heated in a stepwise manner from one predetermined temperature to another. The upper temperature limit of the SALS sample holder was 250 °C.

3. Definitions and Theory

We use a reference volume $\upsilon = 100$ Å^3, which is roughly the volume of a C_4 repeat unit of our components, as the basis for defining the following parameters: the Flory−Huggins interaction parameters χ_{mn} (m, n = A, B, C), the number of reference volume units per chain of each component (N_j), and the statistical segment lengths of the components (l_m), which describe the dependencies of the radius of gyration on N_j. Since the polymer density is temperature dependent, N_j is also temperature dependent.

Our methods for utilizing Flory−Huggins theory (FHT), the random phase approximation (RPA), and self-consistent field theory (SCFT) to describe multicomponent A/B/A−C blends have been previously discussed in refs 4 and 5. The only input parameters needed to utilize these theories are the χ_{mn} and l_m parameters, which have been previously determined from homogeneous binary blends and are tabulated in ref 5. Our SCFT calculations are carried out in 1 dimension, and the effect of concentration fluctuations is neglected. We thus do not differentiate between different microphase-separated states such as microemulsions and lamellae.

4. Results and Discussion

All of the blends discussed in this paper contain the same homopolymers: A is dPB89(24) and B is PIB(24). In addition, the ratio of the volume fractions of A and B homopolymers is fixed; $\phi_A/\phi_B = 0.972 \pm 0.002$. The thermodynamic properties of the binary A/B blend with $\phi_A/\phi_B = 0.972$ are thoroughly discussed in ref 5. This is the critical blend composition, calculated on the basis of the Flory−Huggins theory. At 25 °C, the blend is homogeneous. At 27 °C and above, the blend is macrophase-separated. An interesting property of our A/B blend is that χ_{AB} is nearly independent of temperature. Thus, $\chi_{AB}N_{AVE}$ is only slightly greater than 2.0 in the temperature range of interest ($\chi_{AB}N_{AVE} = 2.04-2.60$ for $T = 27-200$ °C); $1/N_{AVE} = [1/(2N_A^{1/2}) + 1/(2N_B^{1/2})]^2$.

We begin with a description of results obtained by adding the A−C diblock copolymer hPBPB(79−66) to the critical A/B mixture described above. These A/B/A−C multicomponent mixtures are labeled Mxy where xy is the vol % of the hPBPB(79−66) copolymer in the mixture. While we cover a wide range of surfactant concentrations ($\phi_{A-C} = 0.01-0.50$), we are particularly interested in the phase behavior of mixtures with low surfactant concentrations ($\phi_{A-C} = 0.01-0.05$). In this limit, we study the effect of the molecular weight of the surfactant by conducting additional studies on A/B/A−C mixtures with hPBPB(88−93) (series A) and hPBPB(240−192) (series B) as the surfactant. The compositions of all of the multicomponent blends covered in this paper are given in Table 2.

4.1. SANS and SALS Data from A/B/A−C Mixtures Containing hPBPB(79−66). Blend M05, annealed at 150 °C and then cooled to room temperature, showed standard signa-

Table 2. Compositions of Multicomponent Blends

blend	component A	component B	component A−C	ϕ_A	ϕ_B	ϕ_{A-C}
M03	dPB89(24)	PIB(24)	hPBPB(79−66)	0.478	0.492	0.030
M04	dPB89(24)	PIB(24)	hPBPB(79−66)	0.473	0.487	0.040
M05	dPB89(24)	PIB(24)	hPBPB(79−66)	0.468	0.482	0.050
M10	dPB89(24)	PIB(24)	hPBPB(79−66)	0.443	0.457	0.100
M20	dPB89(24)	PIB(24)	hPBPB(79−66)	0.394	0.406	0.200
M30	dPB89(24)	PIB(24)	hPBPB(79−66)	0.345	0.355	0.300
M40	dPB89(24)	PIB(24)	hPBPB(79−66)	0.296	0.305	0.400
M50	dPB89(24)	PIB(24)	hPBPB(79−66)	0.246	0.254	0.500
A03	dPB89(24)	PIB(24)	hPBPB(88−93)	0.478	0.492	0.030
A04	dPB89(24)	PIB(24)	hPBPB(88−93)	0.473	0.487	0.040
A05	dPB89(24)	PIB(24)	hPBPB(88−93)	0.468	0.482	0.050
B01	dPB89(24)	PIB(24)	hPBPB(240−192)	0.488	0.502	0.010
B02	dPB89(24)	PIB(24)	hPBPB(240−192)	0.483	0.497	0.020
B03	dPB89(24)	PIB(24)	hPBPB(240−192)	0.478	0.492	0.030
B04	dPB89(24)	PIB(24)	hPBPB(240−192)	0.473	0.487	0.040
B05	dPB89(24)	PIB(24)	hPBPB(240−192)	0.468	0.482	0.050

tures of single-phase systems. This is shown in Figure 1a where SANS profiles from M05 at selected temperatures between 31 and 130 °C obtained during a heating run are shown. At 31 °C, we see a broad SANS peak at $q = 0.061$ nm^{-1} and a wide SANS plateau at low q. Qualitatively similar data were obtained at 51 °C (data not shown for brevity). The scattering profiles at 31 and 51 °C are very similar to those obtained from periodic microemulsions,[67,68] and we thus use the well-established Teubner−Strey (T−S) equation[67] to analyze the SANS data obtained at these temperatures. The T−S equation for the scattering intensity is

$$I(q) = \frac{1}{a + bq^2 + cq^4} + I_{bgd}(q) \tag{1}$$

where a, b, and c are fitting parameters. We use $I_{bgd}(q)$ to account for the fact the T−S equation was developed for oil/water microemulsions and thus does not account for scattering contributions due to the connectivity of polymer chains. $I_{bgd}(q)$ is assumed to be of the form $I_{bgd}(q) = (eq^2 + g)^{-1}$, where e and g are fitting constants. We do not have rigorous justification for the proposed splitting of $I(q)$. The fitting constants enable determination of the domain spacing, d, correlation length, ξ, and amphiphilicity factor, f_a, given by

$$\xi = \left[\frac{1}{2}\left(\frac{a}{c}\right)^{1/2} + \frac{b}{4c}\right]^{-1/2} \tag{2}$$

$$d = 2\pi\left[\frac{1}{2}\left(\frac{a}{c}\right)^{1/2} - \frac{b}{4c}\right]^{-1/2} \tag{3}$$

$$f_a = \frac{b}{2\sqrt{ac}} \tag{4}$$

The curve through the 31 °C data in Figure 1a shows the least-squares fit to the T−S equation. The T−S parameters obtained from the fit are given in Table 3. Heating the sample to 70 °C results in a significant increase in the low-q scattering, as shown in Figure 1a. However, the scattering profile in the $q > 0.04$ nm^{-1} region is consistent with the T−S equation. The solid curve through this portion of $I(q)$ at 70 °C shows the T−S fit. The increased low-q scattering leads us to conclude that M05 is macrophase-separated at 70 °C. We were unable to determine whether the phase-separated state comprises two or three coexisting phases. The Gibbs phase rule requires the presence of a two-phase region adjacent to the single-phase state. The applicability of T−S analysis to the high-q 70 °C data suggests that one of the macrophases is a microemulsion. This qualitative behavior is also seen at 90 °C (Figure 1a). The SANS profile at 110 °C contains a shoulder at $q \sim 0.04$ nm^{-1}, indicating the possible presence of a periodic phase. However, the data are inconsistent with the T−S equation over the accessible q range. At 130 °C, all evidence of the presence of a periodic phase are lost, and the sample is clearly macrophase-separated (Figure 1a).

In order to confirm that the periodic microemulsion phase at 31 °C (Figure 1a) was the equilibrium morphology, we conducted three separate SANS experiments. In experiment 1, the blend was prepared at 90 °C and transported to NIST at room temperature. When examined by SANS at 31 °C, this sample exhibited the standard characteristics of a phase-separated sample; i.e., the SANS profile was similar to that seen at 130 °C in Figure 1a. Nevertheless, we heated the sample in steps to 200 °C, recorded SANS data wherein phase separation was seen at all temperatures, and then cooled the sample to room temperature. To our surprise, we found that the SANS profile obtained at room temperature was typical of a microemulsion. In order to probe the behavior of M05 further, we conducted experiment 2, in which a new blend of M05 was annealed at 150 °C, transported to NIST at room temperature, and studied as a function of increasing temperature. In experiment 3, the same sample used in experiment 2 was placed back in the SANS instrument and studied a second time as a function of increasing temperature. The data shown in Figure 1a were obtained from experiment 3. The results of experiment 2 are summarized in Figure 1b, where we show $I(q)$. Once again we see a broad primary scattering peak at $q_{SANS-peak} = 0.061$ nm^{-1} at 30 °C. It is worth noting that the location of the primary scattering peak, the width of the primary peak, and the absolute peak intensity obtained from the experiments 2 and 3 are in good agreement. We see some differences at both low and high q. In particular, a second-order peak at $q_2 = 2.8q_{SANS-peak}$ was obtained in experiment 2. We do not know the reason for the appearance of this peak. Heating M05 in experiments 2 and 3 led to macrophase separation above 90 °C. The consistency of the results of experiments 2 and 3 indicates that the equilibrium morphology at 31 °C is a microemulsion. The instrument configuration used for experiment 2 did not allow access to q values low enough to see the incipient signature of macrophase separation seen at 70−90 °C in Figure 1a. T−S fit parameters obtained from experiments 2 and 3 were within 10% at all temperatures. We thus conclude that sample M05 readily attains the equilibrium microemulsion morphology when annealed at 150 °C but not when annealed at 90 °C. The data in Figure 1a show that at 90 °C M05 exhibits complex coexisting phases including a microemulsion, while at 150 °C the sample is completely macrophase-separated. It appears equilibration at 30

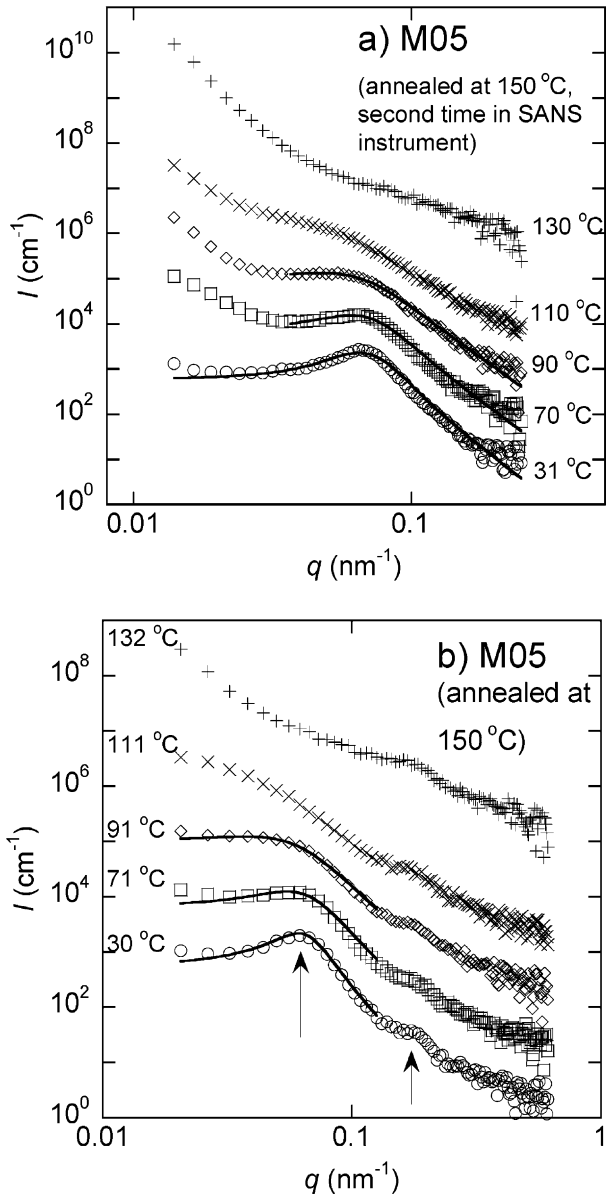

Figure 1. (a) SANS data obtained from blend M05 (annealed at 150 °C, second time heated in SANS instrument, at selected temperatures: 31 (○), 70 (□), 90 (◇), 110 (×), and 130 °C (+). The scattering intensities have been multiplied by the following factors to better delineate the data sets: 10 (70 °C), 10^2 (90 °C), 10^3 (110 °C), 10^5 (130 °C). The solid lines at 31, 70, and 90 °C are the Teubner−Strey scattering profile fit to the data. (b) SANS data obtained from blend M05 (annealed at 150 °C) at selected temperatures: 30 (○), 71 (□), 91 (◇), 111 (×), and 132 °C (+). The scattering intensities have been multiplied by the following factors to better delineate the data sets: 10 (71 °C), 10^2 (90 °C), 10^3 (111 °C), 10^5 (132 °C). The solid lines at 30, 71, and 91 °C are the Teubner−Strey scattering profile fits to the data. The arrows indicate the locations of $q_{SANS-peak}$ and $q_2 = 2.8q_{SANS-peak}$ at 30 °C.

°C is facilitated by starting with the completely phase-separated state at 150 °C.

The M05 sample was uniformly cloudy when observed by the naked eye at room temperature. This is not surprising because the SANS data indicate the presence of a periodic structure with a characteristic length of about 100 nm. This length scale is only a factor of 4 smaller than the wavelength of visible light. We have made similar observations in our previous studies of lamellar and microemulsion phases obtained from A/B/A−C mixtures.[2] Ultra small-angle scattering (USANS) experiments conducted on the BT5 beamline at NIST at

Table 3. Teubner−Strey Fitting Parameters for M-Series Blends

blend	T (°C)	a (cm)	b (cm nm^2)	c (cm nm^4)	d (nm)	ξ (nm)	f_a
M30	90	0.0245	−3.73	153.05	56.39	66.05	−0.963
M30	112	0.0309	−4.30	171.22	55.13	47.72	−0.935
M30	131	0.0347	−4.43	183.37	55.29	34.55	−0.878
M30	150	0.0331	−3.87	182.71	57.30	26.31	−0.787
M20	90	0.0118	−2.15	110.73	62.78	58.43	−0.940
M20	112	0.0128	−2.24	118.59	63.07	45.59	−0.909
M20	131	0.0113	−1.96	120.73	66.66	36.01	−0.839
M10	30	0.0025	−0.69	56.42	78.48	59.50	−0.919
M10	50	0.0022	−0.63	55.67	81.36	55.95	−0.900
M10	70	0.0021	−0.63	60.00	84.15	54.05	−0.887
M10	90	0.0019	−0.60	64.20	88.37	51.39	−0.859
M10	112	0.0014	−0.51	68.43	98.15	49.64	−0.824
M05	30	0.0017	−0.67	88.90	98.87	60.72	−0.862
M05	51	0.0015	−0.54	74.13	98.98	49.73	−0.810
M05	70	0.0014	−0.47	73.20	101.98	41.58	−0.734
M05	90	0.0010	−0.28	72.93	118.26	32.83	−0.518

$T = 30$ °C indicated no signs of macrophase separation in blend M05. Therefore, the lack of optical clarity is related to the large domain size of the microemulsion phase rather than two-phase coexistence. An approximately 100 μm thick sample, when observed in an optical microscope, was featureless and clear at 30 °C, presumably due to the low optical contrast between the PIB-rich and the hPB89-rich phases. In contrast, phase-separated domains were readily observed with the naked eye and in an optical microscope for the M00 binary blend at 30 °C.

SALS data were also obtained from blend M05 (prepared at 150 °C) and are shown in Figure 2. The SALS intensity, which is low at low temperatures, increases abruptly between 50 and 70 °C. This change in the SALS signal is thus correlated with the increase in low-q scattering in the SANS data at 70 °C. A second abrupt change in the SALS signal occurs at $T > 110$ °C. This appears to be correlated to the disappearance of the periodic structure observed in the SANS data. The SALS data provide additional support for our conclusions regarding the phase behavior of M05: microemulsion at $T \leq 50$ °C, macrophase separation in which one of the phases is a microemulsion from 50 °C < T < 110 °C, and macrophase separation without a coexisting periodic structure at $T \geq 110$ °C.

SANS data from blends M03 (annealed at 35 and 150 °C) and M04 (annealed at 90 °C) showed standard signatures of

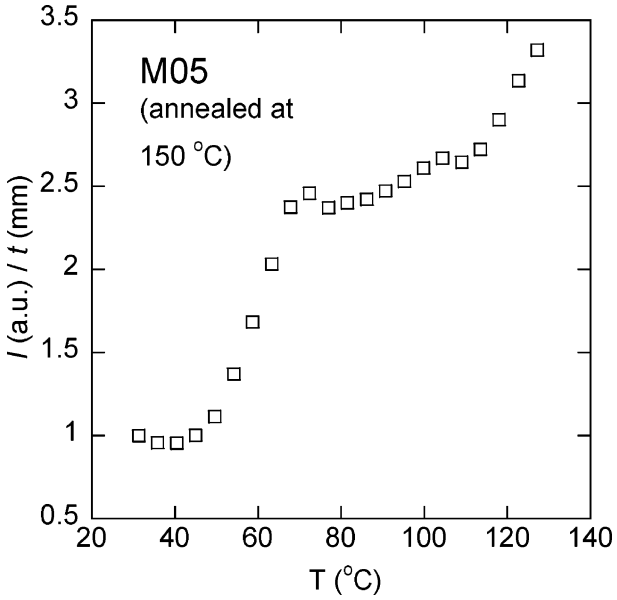

Figure 2. SALS intensity (averaged over a range of q-values and normalized by the sample thickness) is given as a function of temperature for blend M05 (annealed at 150 °C).

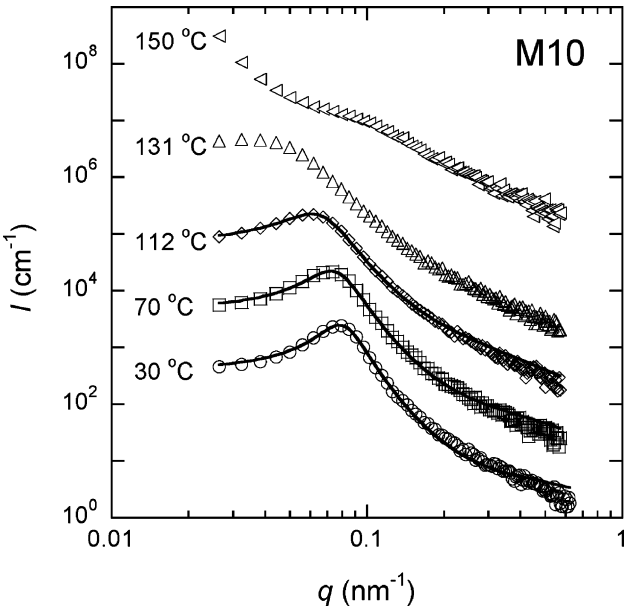

Figure 3. SANS data obtained from blend M10 at selected temperatures: 30 (○), 70 (□), 112 (◇), 131 (Δ), and 150 °C (tilted △). The scattering intensities have been multiplied by the following factors to better delineate the data sets: 10 (70 °C), 10^2 (112 °C), 10^3 (131 °C), 10^5 (150 °C). The solid lines at 30, 70, and 112 °C are the Teubner−Strey scattering profile fit to the data.

macrophase separation at 30 °C. We thus conclude that we need at least 5 vol % of the A−C block copolymer to organize our A/B mixtures, i.e., $\phi_{s,min} = 0.045 \pm 0.005$.

The SANS data obtained from blend M10 at selected temperatures are shown in Figure 3. We obtain a microemulsion phase at temperatures between 30 and 112 °C. The solid curves in Figure 3 show typical T−S fits through the data. The SANS data at 131 °C cannot be fit by the T−S equation. At 150 °C, we see clear signs of macrophase separation. Complementary SALS experiments indicated a macrophase separation transition at 132 ± 5 °C, which is consistent with the SANS data. The SALS data of M10 (and all of the other samples) were consistent with SANS and thus not shown for brevity.

SANS data obtained from blends M30 and M20 are similar. We thus only show SANS data obtained from M30 at selected temperatures in Figure 4a. At 30 °C, we see a sharp primary scattering peak. The peak cannot be fit by the T−S equation. Following arguments in refs 4 and 5, we conclude that M30 has a lamellar phase at 30 °C. We expect a very weak second-order peak corresponding to a lamellar phase due to the symmetric composition of our A/B/A−C blend. Other factors such as the extent of long-range order also affect our ability to detect higher order peaks. Heating M30 to 112 °C results in a significant broadening of the primary SANS peak (Figure 4a), which is consistent with the T−S equation. We take this as a signature of a microemulsion. The microemulsion gives way to a phase-separated state when M30 is heated to 169 °C. The location of the macrophase separation transition was confirmed by SALS.

The ability to observe a higher order peak is often affected by thermal history. After the SANS data shown in Figure 4a were obtained, the blend was then cooled down to −10 °C. The data obtained from blend M30 at −10 °C are shown in Figure 4b. We find a primary and second-order scattering peak corresponding to a lamellar phase. The two peaks persist when the sample is heated to room temperature. This indicates that our conclusion of the existence of a lamellar phase in the preceding paragraph, based solely on the analysis of the primary

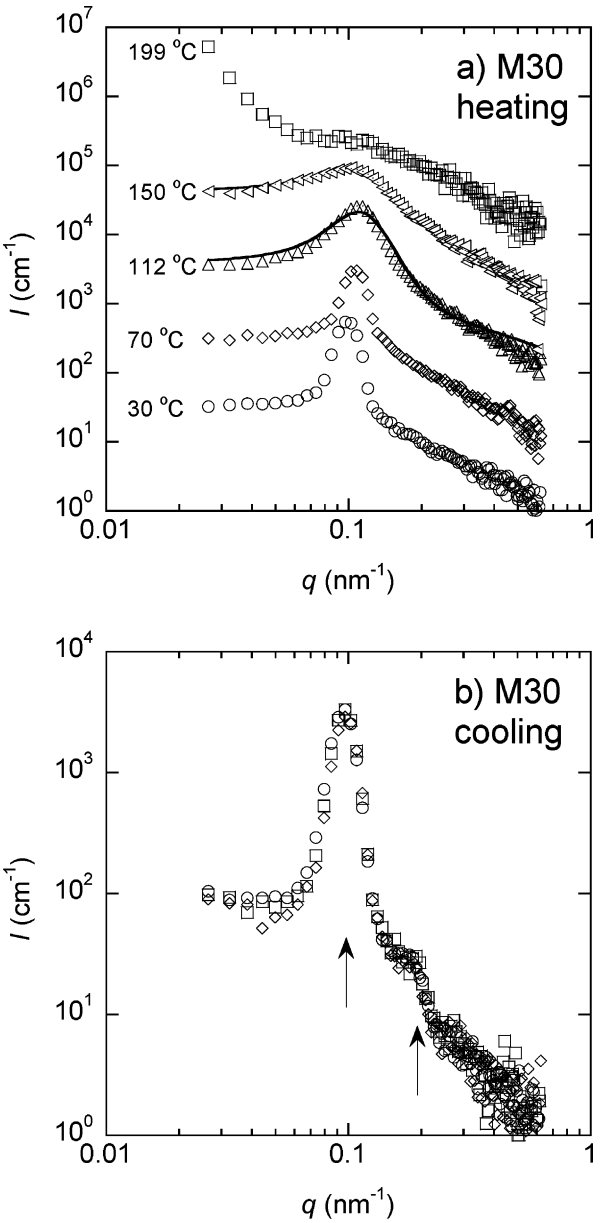

Figure 4. (a) SANS data obtained from blend M30 upon heating at selected temperatures: 30 (○), 70 (◇), 112 (Δ), 150 (tilted △), and 199 °C (□). The scattering intensities have been multiplied by the following factors to better delineate the data sets: 10 (70 °C), 10^2 (112 °C), 10^3 (150 °C), 10^4 (199 °C). The solid lines at 112 and 150 °C are the Teubner−Strey scattering profile fits to the data. (b) SANS data obtained from blend M30 upon cooling: −10 (○), 10 (□), 23 °C (Δ). The arrows indicate the locations of $q_{SANS-peak}$ and $q_2 = 2q_{SANS-peak}$.

SANS peak, is sound. This is important because the thermal history needed to obtain higher order peaks in multicomponent mixtures is not at all obvious. In many cases, e.g., ref 5, we were unable to obtain higher order scattering peaks from A/B/A−C lamellar phases.

The analysis of SANS and SALS data from M40 and M50 are discussed in ref 5. The main difference between blends M40/M50 and M30 is the existence of a homogeneous phase at temperatures between the microemulsion and macrophase-separated states.

In Table 3 we summarize the T−S parameters obtained from all of the microemulsion phases in this series of A/B/A−C mixtures. In Table 4 we give the experimentally determined phase transition temperatures of the mixtures, determined by SANS and SALS. In all cases, we find excellent agreement in

Table 4. Experimental Phase Transition Temperatures (°C) in M-Series Multicomponent Blends[a]

blend	L → M (SANS)	M → P (SANS)	M → P (SALS)
M30	80 ± 10	160 ± 10	164 ± 5
M20	80 ± 10	141 ± 10	151 ± 2.5
M10	NA	121 ± 10	132 ± 5
M05	NA	60 ± 10	52 ± 2.5

[a] L is a lamellar phase, M is a microemulsion phase, and P is macrophase-separated. SANS is small-angle neutron scattering, and SALS is small-angle light scattering.

the microemulsion-to-macrophase separation transition (M → P) temperatures determined from SANS and SALS.

4.2. Comparing Theoretical Predictions with Experiments. One-dimensional SCFT calculations were conducted for blend M05, using methods thoroughly described in refs 4 and 5. All of the χ parameters and statistical segment lengths needed for these calculations are given in ref 5. As shown in ref 5, our calculations distinguish between a homogeneous phase, microphase separation, and macrophase separation, but not between lamellar and microemulsion phases. In Figure 5a we compare the domain spacing d obtained by SCFT with our experimental results for M05. The vertical lines in Figure 5a indicate the location of the experimentally determined phase transitions. The domain spacings based on the SANS data are also shown in Figure 5a (open circles), in which $d_{expt} = 2\pi/q_{SANS-peak}$ where $q_{SANS-peak}$ is the location of the primary scattering peak. The errors on all of the d-spacings determined from SANS reported in this paper are less than 1%. Both experiments and SCFT show a large increase in the d-spacing as the temperature approaches macrophase separation from below. SCFT predicts the formation of periodic phases up to 90 °C. This is in contrast to the experimental results indicating the presence of complex coexisting phases in M05 at temperatures between 70 and 90 °C. Besides this minor disagreement, the agreement between theory and experiment in Figure 5a is remarkably good. In Figure 5b we compare SCFT and experimental d-spacings obtained from M10. Both theory and experiment show an increase in d with increasing temperature up to the macrophase

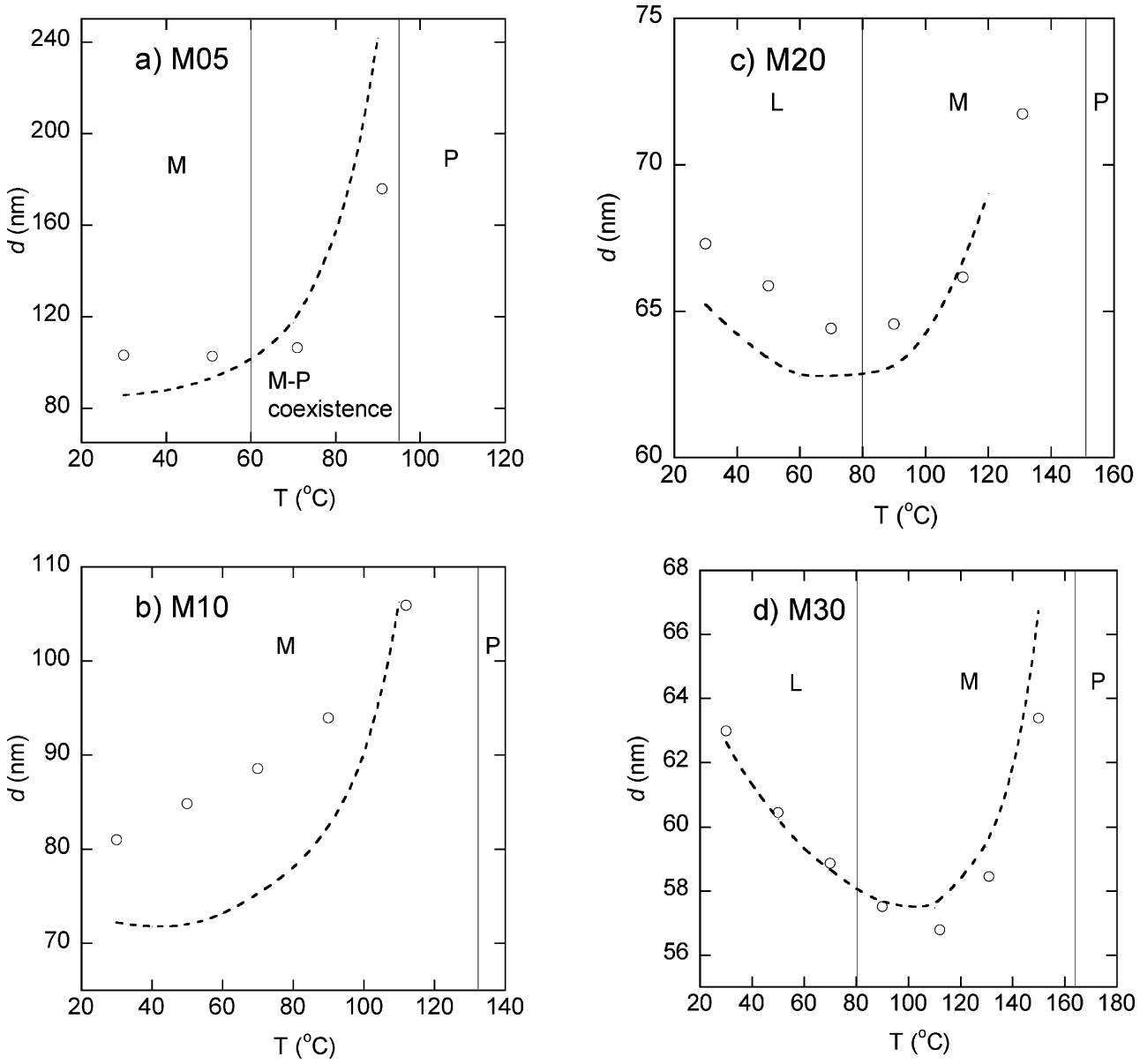

Figure 5. Domain spacing as a function of temperature for blends (a) M05, (b) M10, (c) M20, and (d) M30 as determined by SANS with $d = 2\pi/q_{SANS-peak}$ (○) and predicted by SCFT (dotted line). The vertical lines indicate phase transitions determined from SANS and SALS data. L is lamellae, M is a microemulsion, and P is macrophase-separated.

separation transition. The experimentally observed increase in d from 80 to 106 nm as temperature is increased from 30 to 120 °C is less pronounced than the theoretical predictions. An interesting qualitative change is seen when the surfactant concentration is increased to 20 vol %. As shown in Figure 5c, the experimentally determined d spacing of M20 initially decreases with temperature, reaches a minimum of about 63 nm at 80 °C, and then increases with further increase of temperature. The SCFT calculations capture all aspects of this behavior. In Figure 5d, we show data obtained from M30, which also shows nonmonotonic changes in d with temperature. The statistical segment lengths are weak and monotonic functions of temperature. The nonmonotonic temperature dependence of d seen in Figure 5c,d is entirely due to the fact that χ_{AB} and χ_{AC} decrease with increasing temperature while χ_{BC} increases with increasing temperature.

The location of the microphase-to-macrophase separation transition, T_p, seen in M05−M30 can also be predicted by SCFT. The results of the calculations are similar for all of the samples so we discuss one sample, M30, in detail. We used three different methods to locate T_p:

(1) The equilibrium d-spacing at a given temperature was obtained by imposing a given value of d on the system with appropriate boundary conditions, obtaining the composition profile of the components consistent with those constraints using SCFT, and finally calculating the free energy of the system. The equilibrium value of d is given by one that minimizes the free energy (see ref 4 for details). For M30, at temperatures ≥160 °C, our numerical SCFT scheme did not converge on a profile consistent with the imposed constraints, regardless of the value of d. The inability to reach numerical convergence is most likely due to the formation of a macrophase-separated state. In contrast, we have no problems obtaining convergence at temperatures ≤150 °C, and the results shown in Figure 5d were obtained from these calculations. We thus take 155 ± 5 °C as one estimate of T_p based on the d-spacing method.

(2) In the second method, we compare the free energy of the lamellar phase calculated from SCFT to the free energy of homogeneous and macrophase-separated states calculated with Flory−Huggins theory (FHT).[5] The free energies are not shown for brevity, but a similar analysis was conducted on a different A/B/A−C system in ref 4. At low temperatures (T ≤130 °C), the lamellar phase has the lower free energy, and at high temperatures (T ≥140 °C), the macrophase-separated state has the lower free energy. The free energy of the homogeneous phase is larger than both at all temperatures. Thus, T_p for M30 is 135 ± 5 °C, based upon the comparison of free energies.

(3) The third method involved calculating the interfacial tension γ between the two coexisting phases at temperatures above T_p. Our method for determining γ using SCFT is described in ref 4, and thus γ for blend M30 is not shown for brevity. The formation of high surface area structures such as lamellar phases occurs when the surface tension is vanishingly small. We thus extrapolate $\gamma \rightarrow 0$ to be another indication of the transition to an organized phase. This gives $T_p = 134$ °C for M30.

The above three methods should result in the same value for T_p. The fact that our implementation of the three different methods give three slightly different answers is, perhaps, not surprising, due to the numerical nature of SCFT calculations. Lacking a better alternative, the theoretical estimate of T_p is taken to be the average of these three calculations. For M30, we obtain $T_p = 141 \pm 5$ °C. The experimental value of T_p from SALS for M30 was 164 ± 5 °C. The fact that the experimental and theoretical values of T_p are within 15 °C is reasonable, given the experimental errors in the input parameters χ_{mn}, l_j, and N_j and the assumptions made for the theoretical calculations (1d calculation, use of binary χ's and l's, effect of polydispersity [PDI for all polymers is <1.1], etc.).

Table 5. Microphase[a] to Macrophase-Separated Transition Temperatures (°C) in M-Series Multicomponent Blends

blend	T_p (d-spacing, SCFT)	T_p (γ calculation, SCFT)	T_p (free energy comparison)	T_p average
M30	155 ± 5	134	135 ± 5	141 ± 5
M20	125 ± 5	130	125 ± 5	127 ± 5
M10	115 ± 5	119	115 ± 5	116 ± 5
M05	95 ± 5	104	95 ± 5	98 ± 5

[a] All microphase-separated states are modeled as a lamellar phase with self-consistent-field theory (SCFT). The values of T_p can be compared to the experimental microemulsion to macrophase-separated state (M → P) transition reported in Table 4.

The results of these three methods for calculating T_p for all of the blends discussed above are given in Table 5. In the case of M20, M10, and M05, the values of T_p obtained by methods 1, 2, and 3 are within the precision of our calculations. It is important to note that for these blends the free energy of the lamellar phase was lower than the free energy of the macrophase-separated phase for all temperatures that a domain spacing was converged upon with SCFT. Thus, methods 1 and 2 in these cases give the exact same results. For blends M30, M20, and M10, the theoretically predicted value of T_p (Table 5) is in reasonable agreement with the experimental result (Table 4). For blend M05, the theoretical results predict microphase separation when the experimental data indicate coexistence between a microemulsion and macrophase separation (50−70 °C), and thus the experimental and theoretical determinations of T_p differ.

In the case of blend M03, the interfacial tension calculation, the value of T_p obtained using method 3 was 88 °C. Thus, method 3 predicts the formation of periodic phases at T < 88 °C in M03. However, our SCFT calculations of the d-spacing failed to converge at 30 °C. We only find such gross inconsistencies between the results of the three methods described above when the block copolymer concentration is very low. We do not know the origin of this problem. We speculate that this may be related to numerical difficulties associated with SCFT calculations of periodic phases with very large d-spacings. It is also important to note that experimentally we did not find any evidence of single-phase behavior in M03. It is conceivable that M03 is macrophase separated at equilibrium, and there is a genuine disagreement between the results of method 3 and experiments. It is also possible that the d-spacing of M03 is larger than the upper length scale limit (i.e., low-q limit) of our SANS instrument or that our annealing protocol did not lead to equilibration of M03. It is, perhaps, worth noting that we discovered the annealing history that led to equilibration of M05 by serendipity.

The SCFT results obtained for blends M40 and M50 in this series are discussed in ref 5. In that paper, we only used theoretical method 2 to determine T_p. Method 3 cannot be used due to the presence of an intervening homogeneous phase between the microphase-separated and macrophase-separated states. Extrapolating the temperature-dependent γ values for M40 and M50 to $\gamma = 0$ led to estimates of the phase transition temperatures that were very close to the observed microemulsion-to-homogeneous phase transition temperature, rather than T_p. The proximity of blend M30 to the homogeneous phase might help explain why the three methods of determining T_p

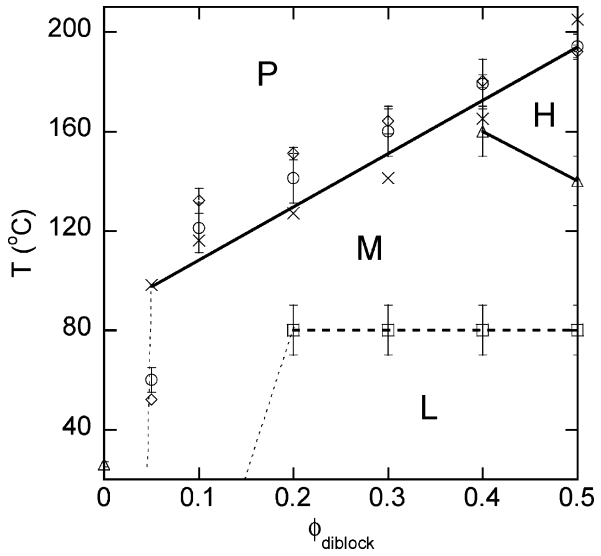

Figure 6. A/B/A−C phase diagram is shown. L = lamellar phase, M = microemulsion, H = homogeneous, and P = macrophase-separated. The phase transition to the macrophase-separated state was determined with both SANS (○) and SALS (◇). The transition from the microemulsion to homogeneous phase was determined with RPA and SANS (Δ). For the binary blend, the transition from the homogeneous phase to macrophase-separated state was determined with RPA and SANS (Δ). The lamellar phase to microemulsion transition was determined with SANS (□). The theoretical calculations of T_p (the microphase-to-macrophase separated transition temperature) are indicated by the × symbols, and a linear fit is indicated by the solid line through the × symbols. Solid lines indicate transitions based upon theoretical calculations. The dashed line (- - -) connects data points from experimentally determined transitions. The dotted lines (•••) indicate phase boundaries determined by comparing blends with different diblock copolymer concentrations at the same temperature.

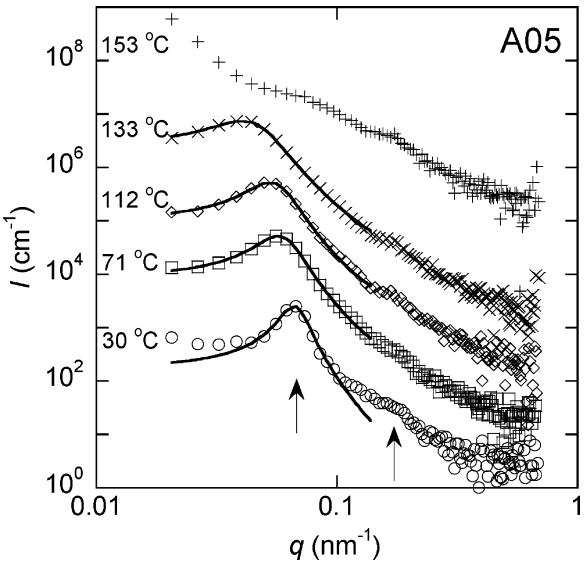

Figure 7. SANS data obtained from blend A05 at selected temperatures: 30 (○), 71 (□), 112 (◇), 133 (×), and 153 °C (+). The scattering intensities have been multiplied by the following factors to better delineate the data sets: 10 (71 °C), 10^2 (112 °C), 10^3 (133 °C), 10^4 (153 °C). The solid lines at 30, 70, 112, and 133 °C are the Teubner−Strey scattering profile fits to the data. The arrows indicate the locations of $q_{SANS-peak}$ and $q_2 = 2.8q_{SANS-peak}$ at 30 °C.

were less in agreement for blend M30 than the other blends (M05, M10, and M20).

The phase diagram of our A/B/A−C system containing hPBPB(79−66) is drawn in Figure 6. The lamellar to microemulsion transitions (squares) were determined utilizing SANS experiments and the T−S equation. Microemulsion to homogeneous phase transitions (triangles) were determined using SANS experiments and the RPA predictions, as described in ref 5. The onset of macrophase separation at elevated temperatures was determined by SANS (circles) and SALS (diamonds). The dashed lines simply connect experimental data. The × symbols represent the theoretical calculation of T_p for blends M05−M50, and the solid line is a linear fit through the × symbols.

While the agreement between theory and experiment in Figure 6 is not perfect, it is clear that the most important experimental result, the addition of hPBPB(79−66) to the phase-separated A/B blend leading to a wide single-phase window that extends all the way to 5 vol % block copolymer, is accurately captured by our theoretical framework.

4.3. Effect of Changing Molecular Weight of Block Copolymer Surfactant. With the success of creating an organized single-phase blend with only 5% of hPBPB(79−66), we examined the possibility of creating blends with even smaller surfactant concentrations. We found that the concentration of surfactant necessary for creating an organized blend was reduced when the molecular weight of the A−C surfactant was increased. The first diblock copolymer we utilized was hPBPB(88−93). We will label blends containing this diblock copolymer as A*xy*, where *xy* is the volume percent of diblock copolymer in the blend. The second diblock copolymer was hPBPB(240−192), and blends containing this diblock copolymer were labeled B*xy*.

The SANS profiles for blend A05 are shown in Figure 7. This blend was annealed at 35 °C. Similar to blend M05, blend A05 was cloudy at 30 °C. We find a strong primary peak (located at $q_{SANS-peak} \sim 0.06$ nm^{-1}) at temperatures ≤133 °C with no evidence of increased low-*q* scattering. In addition, the data in the vicinity of the primary peak were consistent with the T−S equation. Heating A05 from 133 to 153 °C clearly leads to macrophase separation (Figure 7). We thus conclude that blend A05 is single phase at temperatures between 30 and 133 °C. While agreement with the T−S equation is the generally accepted signature of a microemulsion, there is a weak shoulder at $q_2 \sim 2.5q_{SANS-peak}$. We do not have a definitive explanation for this feature. We note that the temperature window over which organized phases are obtained in A05 (30−133 °C) is significantly wider than that of M05 (31−51 °C). Increasing the molecular weight of the A−C surfactant thus increases the window over which organized phases are obtained. Theoretical calculations for T_p were also conducted following the three methods described in this paper, and the average value was 125 ± 5 °C. It is interesting to note that in contrast to blend M05, when blend A05 was annealed in the macrophase-separated state, at 150 °C, we were unable to recover the microphase-separated state at low temperatures. The thermal history that promotes the formation of single-phase morphologies in A/B/A−C blends with 5 vol % block copolymer (or less) was identified entirely by trial and error. In contrast, the structures of blends with ≥10 vol % diblock copolymer were not sensitive to the thermal history.

Blends A03 (annealed at 35 °C) and A04 (annealed at 90 °C) were also studied with SANS but were found to be macrophase separated. This is similar to the results obtained from blends M03 and M04, which were also macrophase separated at all temperatures. Thus, while the larger diblock copolymer increases the temperature window of microphase separation in the 5% diblock copolymer blend, it does not decrease the minimum diblock copolymer concentration needed for forming organized phases. Thus, $\phi_{s,min}$ for both the M-series blends and the A-series blends is 0.045 ± 0.005. Similar to blend M03, the theoretical calculation of T_p for blend A03 was

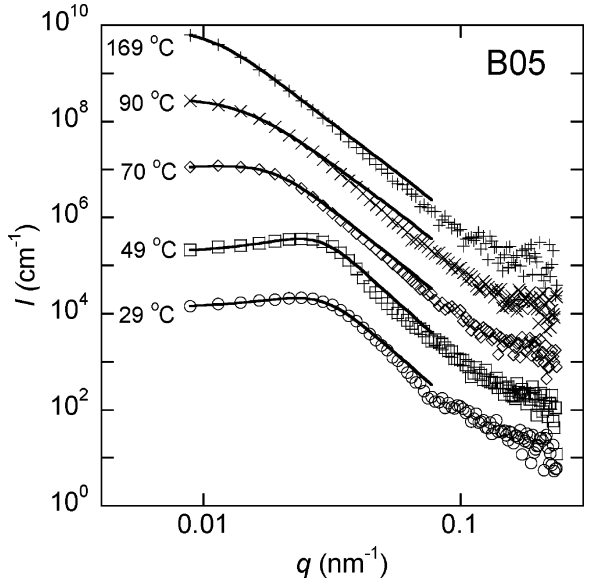

Figure 8. SANS data obtained from blend B05 at selected temperatures: 29 (○), 49 (□), 70 (◇), 90 (×), and 169 °C (+). The scattering intensities have been multiplied by the following factors to better delineate the data sets: 10 (49 °C), 10^2 (70 °C), 10^3 (90 °C), 10^4 (169 °C). The solid lines are the Teubner−Strey scattering profile fits to the data.

Table 6. Microphase[a] to Macrophase-Separated Transition Temperatures (°C) in B-Series Multicomponent Blends

blend	T_p (γ calculation, SCFT)
B05	160
B03	151
B02	146
B01	136

[a] All microphase-separated states are modeled as a lamellar phase with self-consistent-field theory (SCFT).

only possible when utilizing method 3. This calculation resulted in $T_p = 85$ °C.

A series of blends were studied containing 1−5 vol % of the hPBPB(240−192) diblock copolymer. All of these B-series blends were annealed at 90 °C during the sample preparation process. When viewed by the naked eye at 30 °C, all of the B-series samples were significantly clearer than M05 and A05. Blend B05, containing 5 vol % of hPBPB(240−192), was analyzed with SANS, and the resulting data are shown in Figure 8. Clear evidence for the presence of organized microphases is seen between 30 and 70 °C. The SANS profiles for $T = 90$−169 °C were consistent with the T−S equation (data are shown at 90 and 169 °C only in Figure 8 for brevity). However, the primary peak is not seen in the accessible q-window, and thus we are not certain about the structure of B05 in this temperature window. Similar to blends M03 and A03, it was only possible to use method 3 (the interfacial tension calculation) to determine T_p. This is true for all of the blends containing ≤5 vol % of hPBPB(240−192), and thus only method 3 will be discussed for the B-series blends. For B05, $T_p = 160$ °C based upon method 3. The theoretical values of T_p for all of the B-series blends are given in Table 6.

SANS data obtained from blend B01, with 1 vol % hPBPB-(240−192), are shown in Figure 9a. At 30 °C, a periodic microphase is observed. The solid curves in Figure 9a are T−S fits through the data. We thus observe the formation of microemulsions down to 1 vol % block copolymer, i.e., $\phi_{s,min} < 0.01$. To our knowledge, this is the lowest value of $\phi_{s,min}$ obtained. For oil/water mixtures, $\phi_{s,min} = 0.07$ when a single

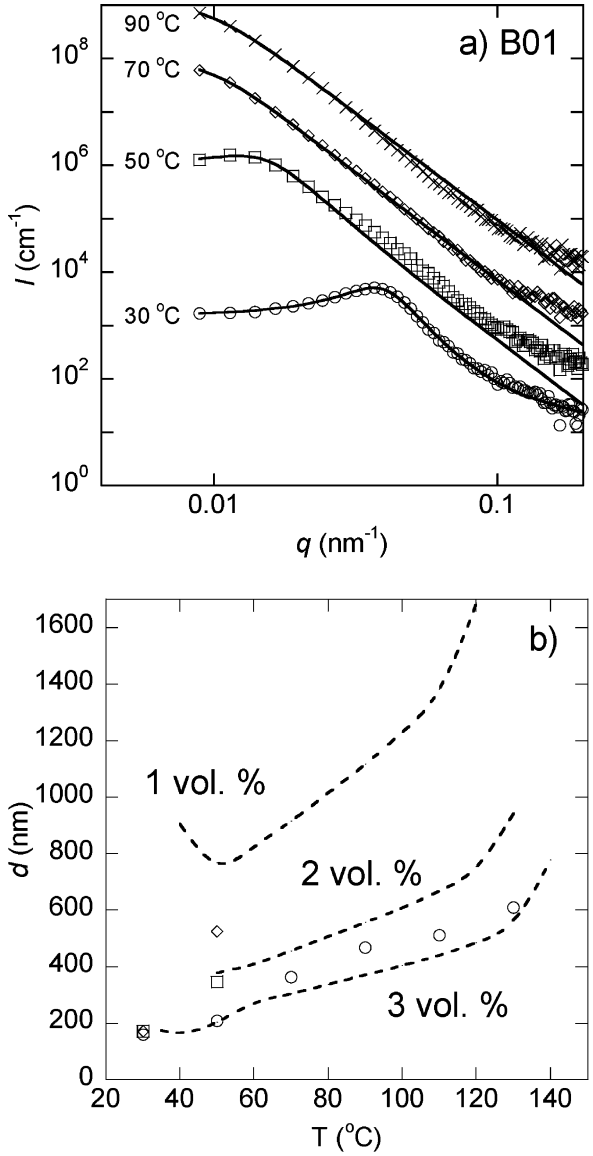

Figure 9. (a) SANS data obtained from blend B01 at selected temperatures: 30 (○), 50 (□), 70 (◇), and 90 °C (×). The scattering intensities have been multiplied by the following factors to better delineate the data sets: 10 (50 °C), 10^2 (70 °C), 10^3 (90 °C). The solid lines are the Teubner−Strey scattering profile fits to the data. (b) Domain spacing as a function of temperature in the microemulsion phase as determined by SANS with $d = 2\pi/q_{SANS-peak}$ (symbols) and predicted by SCFT (dashed curves) for blends B01 (◇), B02 (□), and B03 (○). The domain spacings for all three blends are roughly the same value at 30 °C.

small molecule nonionic surfactant is used[9] and $\phi_{s,min} = 0.03$ when polymer efficiency boosters are added in addition to the small molecule surfactant.[69] For A/B/A−B blends the experimentally determined value of $\phi_{s,min} = 0.09$.[25,26,55] (While theoretical predictions of $\phi_{s,min} < 0.09$ have been made,[43] we are unaware of any experimental results where homogeneous blends are obtained with ϕ_s less than 0.09.) Above 50 °C, a peak is not observed in B01, although the scattering curves are consistent with the T−S equation (solid curves in Figure 9a). Whether this is due to macrophase separation or due to limited q-window of the SANS instrument remains to be determined.

The dashed curves in Figure 9b show the SCFT calculation of the d-spacing for all of the B-series blends as a function of temperature where convergence was obtained. The symbols in Figure 9b are the d-spacings determined from the SANS peak.

At 50 °C, the experimentally determined *d*-spacings increase as block copolymer concentration is decreased. While the *d*-spacing obtained from B01 at 50 °C differs significantly from the theoretical prediction, the overall dependence of *d* on copolymer concentration is in excellent agreement with theoretical predictions. At 30 °C, the experimentally determined *d*-spacings for all three blends were within experimental error. (The values cannot be distinguished from one another in Figure 9b.) We cannot address this finding theoretically due to the lack of convergence of our SCFT calculations. At temperatures above 50 °C, there is excellent quantitative agreement between theory and experiment for the case of B03. For the other samples, we were unable to determine *d* from experiments. It is worth noting, however, that the upper limit of periodic length scales that can be determined by our SANS instrument is 600 nm, and many of the predicted *d*-spacings for B01 and B02 are either close to this limit or exceed it. We thus see large discrepancies between the experimental and theoretical values of the *d*-spacing for most blends with $\phi_{\text{diblock}} \leq 0.05$ in the A-, B-, and M-series blends. It is clear that more complete theories are needed to capture the thermodynamics of A/B/A−C mixtures with low values of $\phi_{\text{A-C}}$.

5. Conclusion

A−C surfactants were designed to organize weakly segregated A and B homopolymers by tuning attractive and repulsive interactions. The minimum concentration of surfactant required to form organized microphases, $\phi_{\text{s,min}}$, was found to be <0.01 for a weakly segregated homopolymer system. This value of $\phi_{\text{s,min}}$ is significantly less than what is observed in A/B/A−B polymer systems as well as oil/water/nonionic surfactant systems. Mean field theories were used to predict the phase behavior and domain size of organized microphases. When $\phi_{\text{diblock}} \geq 0.10$, there was excellent agreement between the theoretical domain size and experiment. With small quantities of diblock copolymer, i.e., $\phi_{\text{diblock}} < 0.10$, the theory underpredicted the size of domains, indicating the need for more complex theoretical models to describe these systems. However, the success of the theory in capturing the phase behavior of the majority of the blends indicates that it can be used as a powerful tool to guide future experiments on designing A−C surfactants for weakly segregated A/B blends. Whether these experimental and theoretical methods will also apply to designing A−C surfactants for highly immiscible homopolymers has yet to be determined.

Acknowledgment. This material is based upon work supported by the National Science Foundation under Grants 0305711 and 0504122. We acknowledge the support of the National Institute of Standards and Technology, U.S. Department of Commerce, in providing the neutron research facilities used in this work.

References and Notes

(1) Lee, J. H. Ph.D. Thesis, Chemical Engineering, University of California, Berkeley, 2002.
(2) Lee, J. H.; Ruegg, M. L.; Balsara, N. P.; Zhu, Y. Q.; Gido, S. P.; Krishnamoorti, R.; Kim, M. H. *Macromolecules* **2003**, *36*, 6537−6548.
(3) Lee, J. H.; Balsara, N. P.; Krishnamoorti, R.; Jeon, H. S.; Hammouda, B. *Macromolecules* **2001**, *34*, 6557−6560.
(4) Reynolds, B. J.; Ruegg, M. L.; Balsara, N. P.; Radke, C. J.; Shaffer, T. D.; Lin, M. Y.; Shull, K. R.; Lohse, D. J. *Macromolecules* **2004**, *37*, 7401−7417.
(5) Ruegg, M. L.; Reynolds, B. J.; Lin, M. Y.; Lohse, D. J.; Balsara, N. P. *Macromolecules* **2006**, *39*, 1125−1134.
(6) Kahlweit, M.; Strey, R. *Angew. Chem., Int. Ed. Engl.* **1985**, *24*, 654−668.
(7) Kahlweit, M.; Strey, R.; Firman, P.; Haase, D. *Langmuir* **1985**, *1*, 281−288.
(8) Kahlweit, M.; Strey, R.; Haase, D.; Firman, P. *Langmuir* **1988**, *4*, 785−790.
(9) Strey, R. *Colloid Polym. Sci.* **1994**, *272*, 1005−1019.
(10) Chen, S. H.; Choi, S. *Supramol. Sci.* **1998**, *5*, 197−206.
(11) Magid, L.; Butler, P.; Payne, K.; Strey, R. *J. Appl. Crystallogr.* **1988**, *21*, 832−834.
(12) Xu, Z.; Jandt, K. D.; Kramer, E. J.; Edgecombe, B. D.; Frechet, J. M. J. *J. Polym. Sci., Part B: Polym. Phys.* **1995**, *33*, 2351−2357.
(13) Shull, K. R.; Kellock, A. J.; Deline, V. R.; Macdonald, S. A. *J. Chem. Phys.* **1992**, *97*, 2095−2104.
(14) Adedeji, A.; Hudson, S. D.; Jamieson, A. M. *Macromolecules* **1996**, *29*, 2449−2456.
(15) Adedeji, A.; Lyu, S.; Macosko, C. W. *Macromolecules* **2001**, *34*, 8663−8668.
(16) Braun, H.; Rudolf, B.; Cantow, H. J. *Polym. Bull. (Berlin)* **1994**, *32*, 241−248.
(17) Ravikumar, H. B.; Ranganathaiah, C.; Kumaraswamy, G. N.; Urs, M. V. D.; Jagannath, J. H.; Bawa, A. S.; Thomas, S. *J. Appl. Polym. Sci.* **2006**, *100*, 740−747.
(18) Tseng, F. P.; Tseng, C. R.; Chang, F. C.; Lin, J. J.; Cheng, I. J. *J. Polym. Res.* **2005**, *12*, 439−447.
(19) Chun, S. B.; Han, C. D. *Macromolecules* **2000**, *33*, 3409−3424.
(20) Jannasch, P.; Hassander, H.; Wesslen, B. *J. Polym. Sci., Part B: Polym. Phys.* **1996**, *34*, 1289−1299.
(21) Cho, K. W.; Jeon, H. K.; Park, C. E.; Kim, J.; Kim, K. U. *Polymer* **1996**, *37*, 1117−1122.
(22) Jannasch, P.; Wesslen, B. *J. Appl. Polym. Sci.* **1995**, *58*, 753−770.
(23) Bates, F. S.; Maurer, W.; Lodge, T. P.; Schulz, M. F.; Matsen, M. W.; Almdal, K.; Mortensen, K. *Phys. Rev. Lett.* **1995**, *75*, 4429−4432.
(24) Hillmyer, M. A.; Maurer, W. W.; Lodge, T. P.; Bates, F. S.; Almdal, K. *J. Phys. Chem. B* **1999**, *103*, 4814−4824.
(25) Bates, F. S.; Maurer, W. W.; Lipic, P. M.; Hillmyer, M. A.; Almdal, K.; Mortensen, K.; Fredrickson, G. H.; Lodge, T. P. *Phys. Rev. Lett.* **1997**, *79*, 849−852.
(26) Washburn, N. R.; Lodge, T. P.; Bates, F. S. *J. Phys. Chem. B* **2000**, *104*, 6987−6997.
(27) Morkved, T. L.; Chapman, B. R.; Bates, F. S.; Lodge, T. P.; Stepanek, P.; Almdal, K. *Faraday Discuss.* **1999**, 335−350.
(28) Cohen, R. E.; Ramos, A. R. *Macromolecules* **1979**, *12*, 131−134.
(29) Datta, S.; Lohse, D. J. *Polymeric Compatibilizers*; Hanser: Cincinnati, OH, 1996.
(30) Hudson, S. D.; Jamieson, A. M. In *Polymer Blends*; Paul, C. B., Ed.; Wiley: New York, 2000; Vol. 1.
(31) Jeon, H. S.; Lee, J. H.; Balsara, N. P. *Phys. Rev. Lett.* **1997**, *79*, 3274−3277.
(32) Jeon, H. S.; Lee, J. H.; Balsara, N. P. *Macromolecules* **1998**, *31*, 3328−3339.
(33) Jeon, H. S.; Lee, J. H.; Balsara, N. P.; Newstein, M. C. *Macromolecules* **1998**, *31*, 3340−3352.
(34) Lyu, S.; Jones, T. D.; Bates, F. S.; Macosko, C. W. *Macromolecules* **2002**, *35*, 7845−7855.
(35) Tan, N. C. B.; Tai, S. K.; Briber, R. M. *Polymer* **1996**, *37*, 3509−3519.
(36) Jackson, C. L.; Sung, L.; Han, C. C. *Polym. Eng. Sci.* **1997**, *37*, 1449−1458.
(37) Sung, L.; Hess, D. B.; Jackson, C. L.; Han, C. C. *J. Polym. Res. (Taiwan)* **1996**, *3*, 139.
(38) Koizumi, S.; Hasegawa, H.; Hashimoto, T. *Macromolecules* **1994**, *27*, 7893−7906.
(39) Kielhorn, L.; Muthukumar, M. *J. Chem. Phys.* **1997**, *107*, 5588−5608.
(40) Balsara, N. P.; Jonnalagadda, S. V.; Lin, C. C.; Han, C. C.; Krishnamoorti, R. *J. Chem. Phys.* **1993**, *99*, 10011−10020.
(41) Leibler, L. *Makromol. Chem., Macromol. Symp.* **1988**, *16*, 1−17.
(42) Leibler, L. *Physica A* **1991**, *172*, 258−268.
(43) Broseta, D.; Fredrickson, G. H. *J. Chem. Phys.* **1990**, *93*, 2927−2938.
(44) Mathur, D.; Hariharan, R.; Neuman, E. B. *Polymer* **1999**, *40*, 6077−6087.
(45) Wang, Z. G.; Safran, S. A. *J. Phys. (Paris)* **1990**, *51*, 185−200.
(46) Janert, P. K.; Schick, M. *Macromolecules* **1997**, *30*, 3916−3920.
(47) Janert, P. K.; Schick, M. *Macromolecules* **1997**, *30*, 137−144.
(48) Muller, M.; Schick, M. *J. Chem. Phys.* **1996**, *105*, 8885−8901.
(49) Maric, M.; Macosko, C. W. *J. Polym. Sci., Part B: Polym. Phys.* **2002**, *40*, 346−357.
(50) Schnell, R.; Stamm, M.; Rauch, F. *Macromol. Chem. Phys.* **1999**, *200*, 1806−1812.
(51) Zhao, H. Y.; Huang, B. T. *J. Polym. Sci., Part B: Polym. Phys.* **1998**, *36*, 85−93.
(52) Ruzette, A. V.; Leibler, L. *Nat. Mater.* **2005**, *4*, 19−31.

(53) Tanaka, H.; Hasegawa, H.; Hashimoto, T. *Macromolecules* **1991**, *24*, 240−251.
(54) Messe, L.; Corvazier, L.; Ryan, A. J. *Polymer* **2003**, *44*, 7397−7403.
(55) Morkved, T. L.; Stepanek, P.; Krishnan, K.; Bates, F. S.; Lodge, T. P. *J. Chem. Phys.* **2001**, *114*, 7247−7259.
(56) Thompson, R. B.; Matsen, M. W. *J. Chem. Phys.* **2000**, *112*, 6863−6872.
(57) Werner, A.; Schmid, F.; Binder, K.; Muller, M. *Macromolecules* **1996**, *29*, 8241−8248.
(58) Shull, K. R.; Mayes, A. M.; Russell, T. P. *Macromolecules* **1993**, *26*, 3929−3936.
(59) Flory, P. J. *J. Chem. Phys.* **1941**, *9*, 660.
(60) Huggins, M. *J. Chem. Phys.* **1941**, *9*, 440.
(61) Benoit, H.; Benmouna, M.; Wu, W. L. *Macromolecules* **1990**, *23*, 1511−1517.
(62) Akcasu, A. Z.; Tombakoglu, M. *Macromolecules* **1990**, *23*, 607−612.
(63) de Gennes, P. G. *Scaling Concepts in Polymer Physics*; Cornell University Press: Ithaca, NY, 1979.
(64) Glinka, C. J.; Barker, J. G.; Hammouda, B.; Krueger, S.; Moyer, J. J.; Orts, W. J. *J. Appl. Crystallogr.* **1998**, *31*, 430−445.
(65) Kline, S. NIST Center for Neutron Research, 2001.
(66) Balsara, N. P.; Lohse, D. J.; Graessley, W. W.; Krishnamoorti, R. *J. Chem. Phys.* **1994**, *100*, 3905−3910.
(67) Teubner, M.; Strey, R. *J. Chem. Phys.* **1987**, *87*, 3195−3200.
(68) Chen, S. H.; Chang, S. L.; Strey, R.; Samseth, J.; Mortensen, K. *J. Phys. Chem.* **1991**, *95*, 7427−7432.
(69) Gompper, G.; Richter, D.; Strey, R. *J. Phys.: Condens. Matter* **2001**, *13*, 9055−9074.

MA0612677